PERFORMANCE EVALUATION OF BUILDING PHOTOVOLTAIC DOUBLE-SKINS

Leon Gaillard[1], Christophe Ménézo[1], Stéphanie Giroux[2], Hervé Pabiou[2], Rémi Le Berre[3]
[1] Chaire INSA de Lyon/EDF, Centre de Thermique de Lyon CETHIL UMR 5008, « Habitat et innovations Energétiques », 69621 Villeurbanne, France
[2] Centre de Thermique de Lyon, CETHIL UMR 5008 UCB Lyon1/CNRS/ INSA, France
[3]Electricité de France R&D, Département ENERBAT, Les Renardières, 7700 Moret sur Loing, France

ABSTRACT

Naturally ventilated, PV active double skin facades can contribute to both the thermal performance of a building and its electrical energy demand. In such systems, the stack effect is exploited to extract heat from PV modules installed on the outer surface. By cooling PV components, electrical performance is improved, and the air drawn through the cavity by natural convection may be used for ventilation or as a form of dynamic insulation. In order for their energetic utility to be fully realised however, their thermal performance must be demonstrated, and a greater understanding of design best practices be developed. In this paper, we present an evaluation of the thermal behaviour of three full-scale prototypes developed as part of the Ressources project. An experimental approach is adopted to reveal qualitative differences between the performance of each system. The causal relationship between environmental conditions and thermal response is studied using a linear parametric model fit to short sequences of data using multivariate regression and then extrapolated to similar days in the same year.

INTRODUCTION

The building sector accounts for a large portion of total energy consumption in many European nations. Thus in the context of current targets to reduce greenhouse gas emissions by a factor of 4 by 2050 compared to 1990, and a 20% reduction by 2020 whilst increasing by 20% the share of renewable energy (EC, 2010), improvements to building energy efficiency can contribute significantly to national objectives. Regulations in France will require new buildings from 2020 to be energy-positive (BEPOS) (MEDDE, 2012). This necessitates improvements to insulation, passive energy storage, and air-tightness, but also a diversification of electrical and thermal energy production, and co-generation solutions. This implies a redefinition of the envelope (roof and facades) conventionally concerned with insulation and sealing, to include dynamic (seasonal or daily variation) and active features (energy production and augmented ventilation). Building-integrated photovoltaic (PV) systems offer local electricity generation and temperature control by natural or forced convection. The inherent heating of crystalline silicone cells can be overcome by natural (BIPV) or forced (PV-T) convection (Chow, 2010). The performance of such integrated PV systems is highly sensitive to the design, and since the demand for PV systems fully integrated into the building frames (facade, roof) is still quite recent, few studies are currently available on the subject.

The Ressources project aims to advance the understanding of double-skin configurations. Three prototypes were designed: one for an existing office building facade and two for detached houses. In this paper, we examine the thermal behaviour of these first three prototypes constructed for the Ressources project. In the first part of the results section, a comparative evaluation of the 3 prototypes is presented, which focussed on the instantaneous response during a typical sunny day in summer. In the second part, system predictability is tested by comparing measured heat extraction to a prediction obtained from an empirical model.

Figure 1 : prototype PV double-skin façades constructed at the ETNA laboratory, EDF, Moret sur Loing. Left: ETNA B. Right: ETNA A.

EXPERIMENT

Photographs of the three prototypes are shown in figures 1 and 2. The prototypes comprise three different geometries of double skin structures with integrated, glass-backed, coloured PV modules. Natural ventilation driven by the stack effect in the

air gaps is expected to cool the PV arrays. At the EDF R&D Renardières site, Moret sur Loing, France, two PV double-façades were installed on the S.S.W. facing wall of the ETNA laboratory. This building comprises a pair of test cells, identical in terms of their thermal characteristics (Neymark et al., 2005).

The ETNA A and B prototypes each include PV cladding covering a section of the wall and roof of the building. The former is a façade/rooftop configuration with a constant depth air gap of 70 cm. ETNA B, is a veranda/rooftop configuration that offers an additional living space of 12m². The rooftop section of ETNA B is less inclined than the underlying rooftop, producing an air gap, which reduces with height to 43.6cm at the upper outlet. The façade portion of each PV-T measures 5.6 m in height and 3 m in width. The PV arrays of ETNA A and B have rated powers of 3.3 and 3.8kWc respectively.

Figure 2 : Double-skin PV prototype from RESSOURCES installed at HBS-Technal, Toulouse

A third PV active double skin façade was installed on an existing occupied tertiary building situated in Toulouse, France. Designed for a facade obliquely oriented to south, the HBS prototype comprises a series of adjacent prism structures with PV modules incorporated into the more southerly-oriented surfaces. The double-facade is 7.40m tall and 4m wide, and positioned to give an air gap of 60cm to 80cm, with openings to the exterior at the upper and lower ends of the structure. PV components are arranged into a vertical stack of three independent arrays or "blocs" with a combined peak power of 1.2kW. The glazed primary wall visible in the photo is identical to the section behind the prototype.

The apparatus was equipped to monitoring the electrical, aerodynamic and thermal behaviour of the prototypes as a function of environmental conditions continuously for a period of one year. Figures 3 and 4 present the instrumentation for the three prototypes. For temperature measurements, 1mm diameter K-type thermocouples (protected from radiation by aluminized pellets) were fitted to surfaces and in the air gaps in the central section of each prototype. Vertical air velocities within the range [0.05,2] m/s were measured using Ahlborn FV1935 TH4 anemometers. Each site was additionally equipped with a weather station that included pyranometers for horizontal and in-plane radiation measurements, a pyrheliometer for the direct component, and sensors for ambient air temperature, wind conditions, humidity and air pressure.

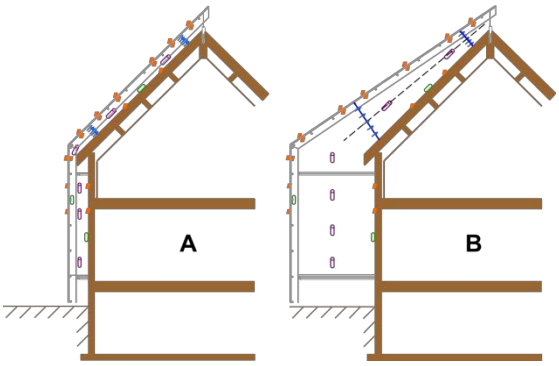

	Sensor	ETNA A	ETNA B
→	Air velocity	2 x 5	2 x 5
▮	Surface temperature	PV ext. 9 PV int. 7 Roof 2 Wallext. 2	PV ext. 9 PV int. 7 Roof 2 Wall ext. 2
▯	Air temperature	6	6
⬭	Hygrometer	3	3
◎	Pyranometer	2	1

Figure 3 : Position of main sensors on ETNA prototypes

For the HBS prototype, sensors were governed by a data acquisitions system connected to a Keithley 3706 data logger and two Almemo cards. A data acquisition (DAQ) programme was developed with Labview to read all instruments in a single loop once every 120seconds for the HBS prototype. The DAQ was managed remotely via a VNC interface. The ETNA prototypes were monitored locally. Prior to the analysis, raw data from all prototypes were imported into a bespoke MySQL database. Scilab, the open-source software, was used to interface with the database directly and perform analyses comprising both structured data queries and matrix manipulation of retrieved data (Scilab, 2012).

Depending on the specific geometry of the prototypes, spatial average measures were calculated to obtain effective mass flow rates. The weighted

average of individual readings was used, with a weighting derived from the effective cross-sectional area of the cavity attributed to each sensor. Such a weighting was chosen to minimise errors that would result from a steep velocity profile in a given horizontal section. The vertical mean air temperature was estimated from the average temperatures per bloc and the ambient (inlet) air temperature by interpolating between each value and calculating a centroid of the resulting distribution.

Heat recovery by the air cavity was calculated as the product of measured mass flow rate, specific heat capacity and measured air temperature difference between outlet and inlet. Mass flow rate was derived from the spatial average air velocity and the local air density, approximated from a standard equation for humid air, using atmospheric conditions measured by the weather station and the spatial average air temperatures

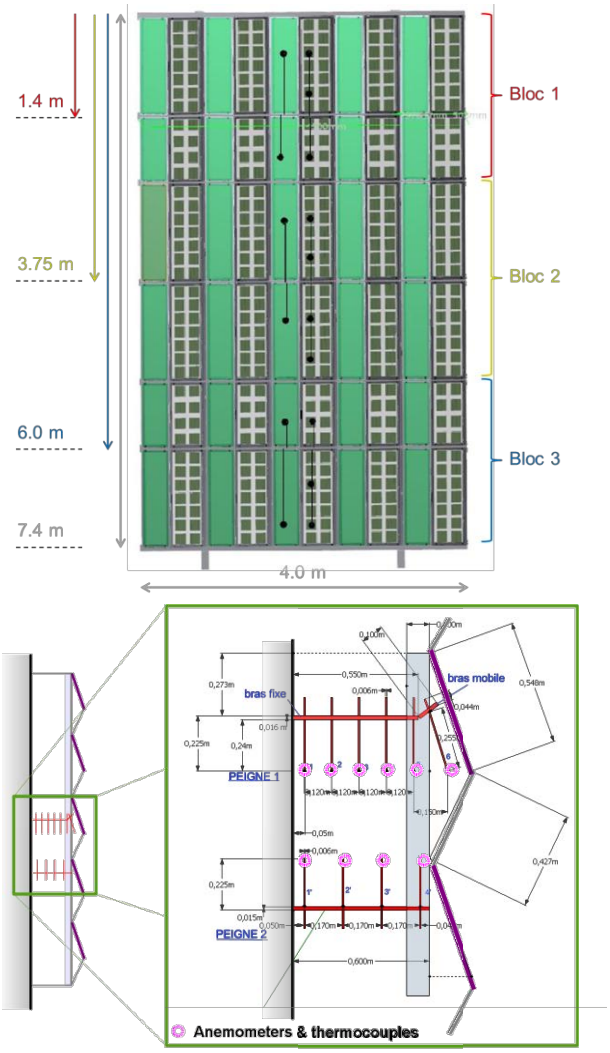

Figure 4 : Position of main sensors on the HBS-Technal prototype. Top: view of the façade façade. Down : view from the top of the façade – section with sensors

In addition to the solar heat source, the building may make a significant contribution to the heat flux entering the cavity. In order to evaluate the apparent contributions of these two sources, a simple energy balance equation was adopted following the approach presented by (Zollner et al. 2002). As for the case of a box window in that study, here the heat recovery of the double skin façade is assumed entirely accounted for by exchanges with the PV façade and the building primary skin, defined in terms of a global heat transfer coefficient and surface-air temperature differences. Equating the heat fluxes with the net enthalpy change of the cavity (recovered heat), and assuming common surface areas and heat transfer coefficients for each contribution, Equation (1) is obtained.

$$mC_p\Delta T_{air} = hA\left(\left(T_e - T_f\right) + \left(T_b - T_f\right)\right) \quad (1)$$

$$\Rightarrow h = \frac{\dot{m}C_p\Delta T_{air}}{A\left(T_e + T_b - 2T_f\right)}$$

where ΔT_{air} is the temperature difference between inlet and outlet, subscripts e, f and b denote the outer facade, cavity air, and building wall respectively, h is a convective heat transfer coefficient and A the surface over which heat is transferred. Note that direct coupling to incident radiation (semi-transparency of PV façade), and wind effects are neglected, as is any mass transfer with the building interior. Hence, a simple relation involving air and surface temperatures provides an estimate of the heat flux from each source.

A comparative evaluation of the three prototypes was performed by considering their respective response to similar environmental conditions. In the following section, the thermal behaviour of the HBS, ETNA A and ETNA B prototypes is presented for a typical sunny day. A preliminary study of the causal relationship between system inputs (environmental factors) and outputs (for example, heat extraction by the cavities) was also undertaken, with the aid of an empirical model.

RESULTS

Comparative evaluation of behaviour

The database was queried to retrieve typical days in terms of the measured environmental conditions. From a sample of 133 days from 25/06/2012 to 5/11/2012 where all 3 prototypes were operated in "summer" configuration, sunny days with little mean wind were identified using aggregated queries. This subset of days was then further filtered to obtain similar days for the two sites. By this method, the data in figures 5 were selected, which describes the evolution in environmental conditions and system behaviour during 9/09/2012 (in general the selected could be from different days for the two sites). On this day, the cumulated direct solar radiation was

6.93 kW/m² for the ETNA site and 6.88 kW/m² for HBS. The horizontal total radiation was also similar: 5.56 kW/m² and 5.50 kW/m² for ETNA and HBS respectively. The variation in ambient temperature for the two sites were similar but not identical. At ETNA the ambient air temperature varied in the interval [10.5, 32.6] °C whereas at HBS the variation was [16.8, 31.7] °C.

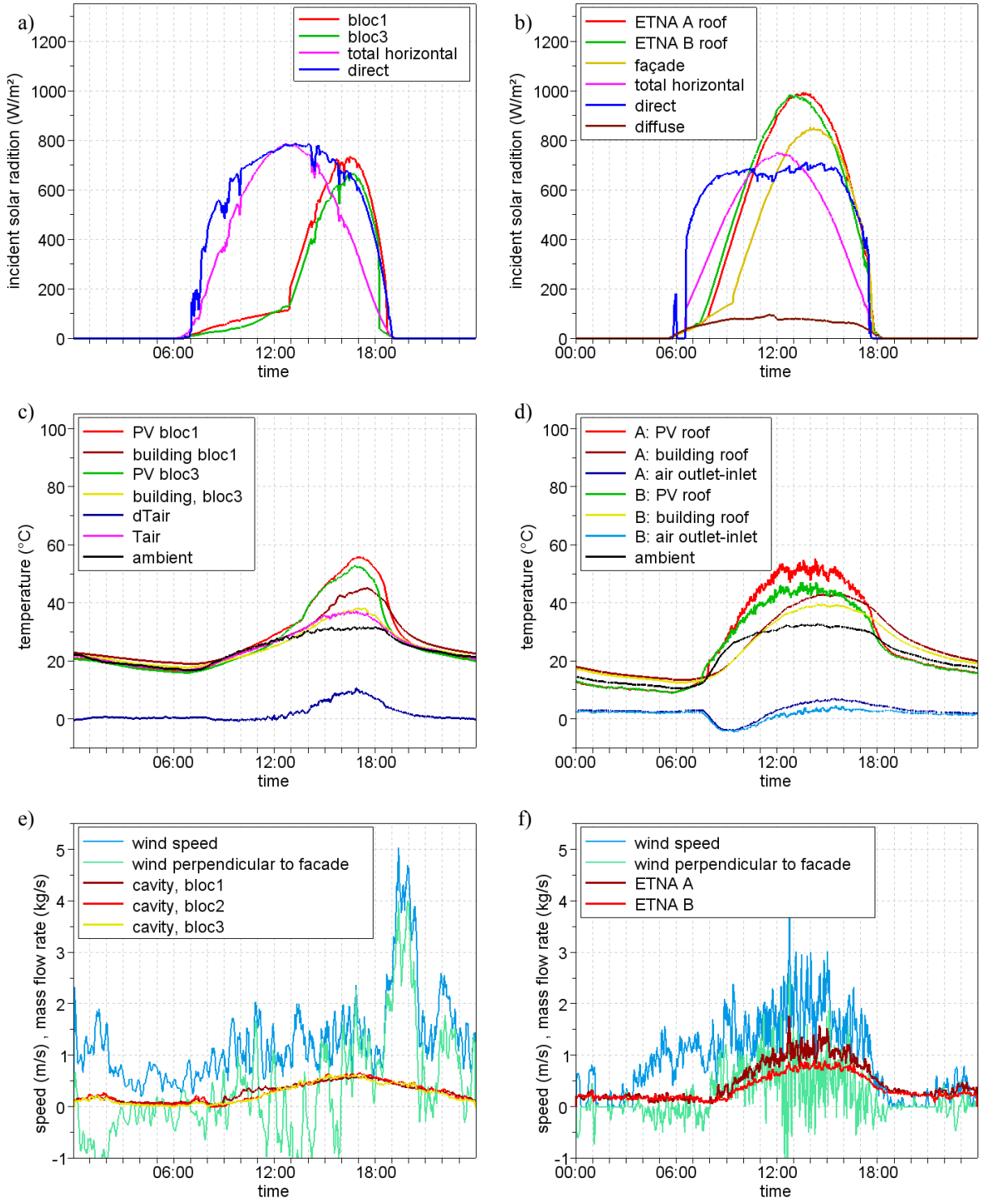

Figure 5 : incident solar radiation, temperatures, wind speed and mass flow rates for one typical sunny day. Left frames: HBS prototype. Right frames: ETNA A & B prototypes

As can be seen in figures 5, the behaviour of the three prototypes is centred on the afternoon as a result of the southwesterly orientation of the systems. Peak incident radiation for the HBS site occurs around 17:00 for the selected day. For the rooftop sections of ETNA A and B, peaks occur at 13:00 and

13:30 (the difference due to their inclinations). The temperature evolution of the surfaces and air is summarised in figures 5c) and 5d). As expected, PV temperatures are correlated with radiation. In contrast, the peak temperature of the building primary façade appears delayed by ~1 hour for all prototypes. Note that, despite a more intense incident radiation for ETNA, the mean array temperatures are similar to the HBS façade. This observation is consistent with the stronger stack-induced flow that is observed to develop for the ETNA prototypes (despite the shallower inclination). The fluctuation in temperatures is less pronounced for HBS.

The HBS and ETNA prototypes also differ in terms of the temperature of outlet air and the mass flow rate. For HBS (fig 5c), the temperature difference data (outlet - ambient) remains positive throughout the day. After passing a maximum of ~10 °C around the time of peak radiation, it is observed to decrease more gradually than the fall-off in radiation, a delay that can be accounted for by heat flux from the building. A qualitatively different trend is apparent for the two ETNA prototypes (fig 5d): rather than increasing, dT_{air} is negative during the morning while the facades are still in shade but the rooftop is irradiated. A minimum of -5 °C is observed around 9:00 for both structures. This trend is reversed once the facades are directly illuminated by sunlight, from which time the trend appears to follow incident radiation until achieving a maximum of +7°C at 16:00 for ETNA A and +4°C for ETNA B.

The mass flow rate is shown in figures 5e) and 5f) for the same selected day, with wind speed measurements superposed. The data have been smoothed with a period-5 moving average filter. The largest observed mass flow rate is for ETNA A, which also exhibits the largest degree of fluctuations. During the daytime, air flow is generally weakest in the HBS prototype. This is consistent with the fact that this façade is the least opaque (a smaller proportion of its surface incorporates PV cells). However, in contrast to the other systems, the mass flow rate in the HBS double façade is observed to persist for a significant period after sunset. During a previous analysis of the HBS façade, this behaviour has been linked to an injection of heat from the building to the air gap (Gaillard et al., 2012).

Figure 6 presents the evolution in extracted heat for the air cavities of the three prototypes. The estimated heat flux from the PV façade and the primary building façade are superposed on the same axes. The HBS prototype is observed to attain a peak heat extraction of 5.0±0.1 kW at 17:00, corresponding to an instantaneous thermal efficiency, the ratio of total heat recovered by the cavity air to the incident solar power (Ong et al., 2003), of 24.7±4.9%. The behaviour of ETNA A during the afternoon is similar to HBS, although the heat gain is observed to fluctuate considerably. The prototype achieves a peak extraction of 8.0±2kW, equivalent to an instantaneous thermal efficiency of 42.8±10.7%. Therefore, the air gap of the ETNA A prototype is a more effective at cooling the PV façade than the HBS configuration. In terms of heat extraction by the cavity, ETNA B is inferior to the other prototypes, reaching a peak heat transfer of 2.5±1kW, equivalent to a thermal efficiency of 11.3±4.5%. Fluctuations are more important for ETNA B than HBS.

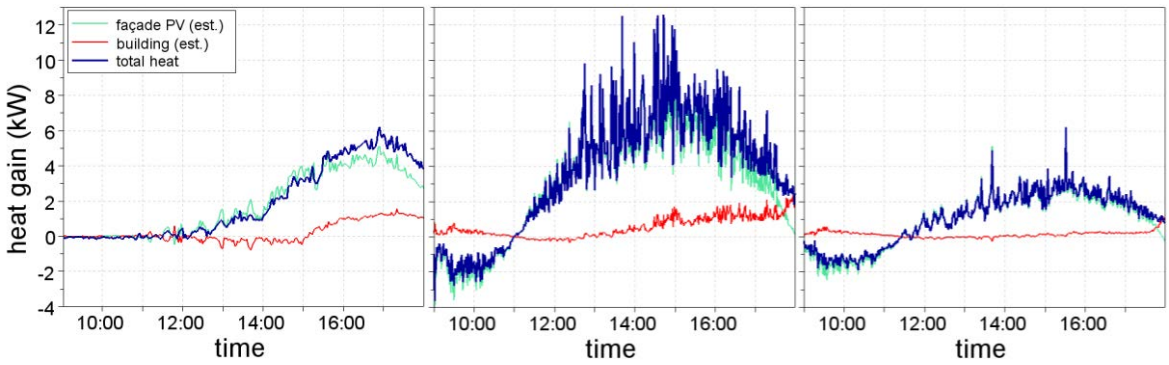

Figure 6 : heat extraction by the double façade air cavity, and the estimated heat fluxes from the PV façade and building primary wall. From left to right: HBS, ETNA A, ETNA B.

Empirical model development

Behaviour models for heat recovery were based on a consideration of energy balance and observed correlation features. For each model, parameter identification was performed by constructing a design matrix and calculating the least square solution by the standard analytical solution for multiple (ordinary) linear regression.

Rather than searching for an optimal model to predict the response of the prototype, the objective was to assess the general validity of such an approach, whilst testing the hypothesis that a stationary linear model is appropriate for the case in study. If proven robust, the method offers a first order prediction of system performance without a prior knowledge of the

physical properties of each component, nor the specific geometric of the structure.

Equation (2) describes the energy balance of the outer façade of the double skin structure, assuming negligible thermal mass. Similar approximations have previously been used in simulations of PV-T collectors, for example (Guiavarch et al., 2006, Chow et al. 2003). The net heat recovered by the cavity air from all sources, Q_g, is defined in terms of the independent variables ambient temperature Ta, façade temperature T_e, building wall temperature T_b, incident radiation G_i, and the sky temperature T_s:

$$\frac{Q_g}{A} = \left[h_{conv,ext} + h_{rad,ext}\right](T_a - T_e) + \left[h_{rad,ext}\right](T_s^4 - T_a^4) + \left[h_{rad,int}\right](T_e^4 - T_b^4) + \left[\alpha\left(1 - \frac{\eta}{\alpha}\right)\right]G_i \quad (2)$$

The plane projection of the outer surface was used for the effective area A. A similar description of thermal behaviour was used to study the performance of rooftop BIPV systems (Guiot 2012). The first two terms on the right hand side of the equation represent the convective and radiative coupling to ambient air and sky. Radiative exchange within the cavity is accounted for by the third term. The last term describes the incident solar energy flux. The model coefficients, shown enclosed by square braces in the above equation, are related to the physical properties of the system. The absorptivity of the outer PV façade is given by α, the photo-conversion efficiency of PV modules is described by η, $h_{conv,ext}$ the convective heat transfer coefficient to the exterior (coupling to the ambient air temperature), and $h_{rad,ext}$ & $h_{rad,int}$ describe radiative heat transfer from the double skin wall to the sky and to the building wall respectively. All were assumed constant to first order. Solutions were not improved by modulating external convection by measured wind speed; hence, this dependence was excluded from the model. External convective and radiative terms were grouped in order to reduce sensitivity to T_s, which was approximated from ambient temperature using the relation

$$T_s = T_a \varepsilon_s^{0.25} \quad (3)$$

where temperatures are in Kelvin, and the sky emissivity ε_s is a function of relative humidity and the dew-point temperature.

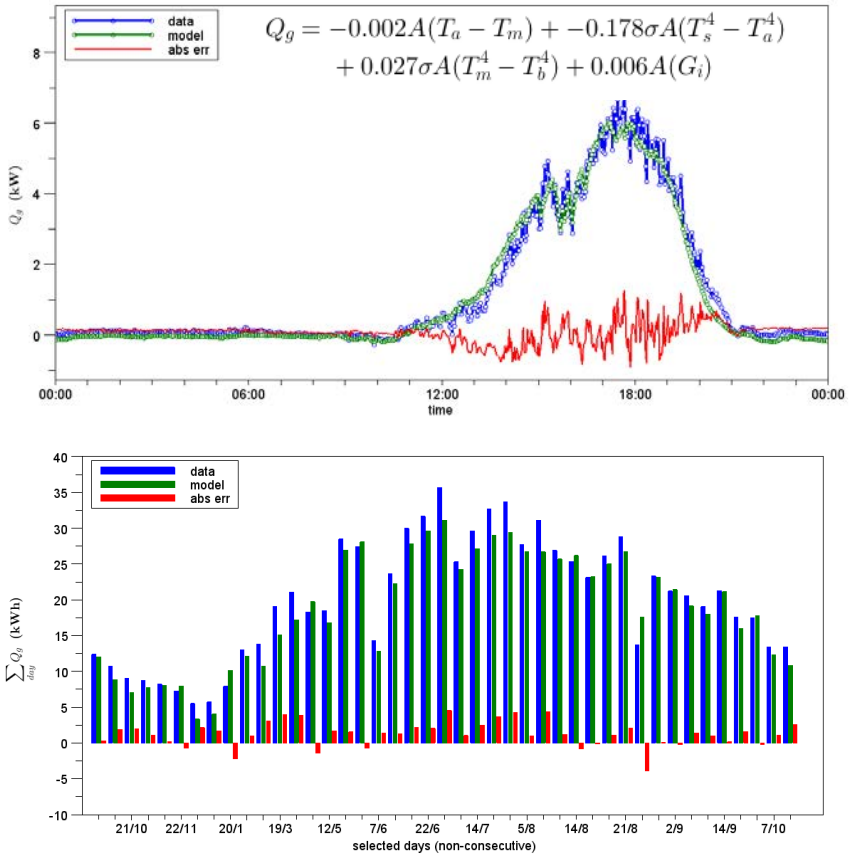

Figure 7: Least square solution of a linear parametric model for heat recovery as a function of measured environmental conditions and facade surface temerpatures. The bar chart illustrates an extrapolation of the solution in summer to one year.

The parametric model for heat recovery was solved using a dataset of 10 sunny summer days with little wind. In figure 7a), the solution is shown superposed over experimental data for one of these days. In general, the model faithfully reproduces the daily trend in heat recovery. Since the model is stationary, short-term fluctuations in the data are not predicted by the model. The inclusion of transient behaviour would require modifications to the model, such as the inclusion of autoregressive terms. Other anomalous features were found to correlate with electricity generation and not pyranometer readings. The uncertainties associated to local meteorological conditions are therefore an important source of error to predictions.

The solution for sunny days in summer was extrapolated to predict performance during similar days spanning one year. In figure 7b), a comparison of measured and predicted daily cumulated heat recovery is presented together with the absolute error. For most days, the prediction is accurate to within 3 kWh, and in general underestimates heat recovery. Absolute errors are not strongly correlated with the cumulated energy; hence relative errors tend to be more significant in winter. The model-data comparison shows that the double skin façade behaves in a consistent and predictable manner throughout the year for days with little wind. A simple stationary model is able to forecast daily heat recovery to mean precision of 6.7% for the available dataset.

CONCLUSION

We have presented the first experimental observations of innovative building double-skins PV, with natural convection corresponding to a summer operational mode. Despite significant uncertainties in the exact state of each system operating under real conditions, clear trends in behaviour are observed.

The regularity in thermal response suggested by daily cycles was verified by the parametric analysis of the data with an empirical model: heat extraction by the cavity is reasonably well described by a linear model composed of few independent variables. This is a significant result, given the complexity of real operating conditions and limited information regarding the physical properties of the double skin façade. Indeed, the coefficients derived by the model implicitly include this information, and the uncertainties on their values are inherently linked to the assumption that they are time-invariant. Future studies could be directed to the experimental determination of physical parameters. Trials using other model formulations, such as with wind speed as an explanatory variable, were not found to improve the quality of the model. However, a systematic approach is required to vindicate the choice of model, or indeed improve it. Therefore in further work, the relationships between system inputs and outputs shall be more rigorously explored using data mining techniques that allow a more rigorous analysis of all observed correlations.

NOMENCLATURE

m = air mass flow rate at the exit of the gap (kg/s)
C_p = air specific heat (J/(kg.K))
ΔT_{air} = air temperature difference between inlet and outlet of cavity (°C)
h = overall heat transfer coefficient (W/m²/K)
A = equivalent surface area for heat transfer (m²)
T_e = mean temperature of outer (PV) facade (°C)
T_f = mean temperature of air in cavity (°C)
T_b = mean temperature of inner façade (building primary wall) (°C)
Q_g = heat extracted by cavity, defined by enthalpy change (W)
$h_{conv,ext}$ = convective heat transfer coefficient to exterior (W/m²/K)
$h_{rad,ext}$ = radiative heat transfer coefficient to exterior (W/m²/K)
T_s = sky temperature (°C)
T_a = exterior ambient temperature (°C)
$h_{rad,int}$ = radiative heat transfer coefficient inside the cavity (W/m²/K)
α = absorptance of PV modules (-)
η = solar cell operating efficiency (-)
G_i = incident solar radiation flux (W/m²)
ε_s = emissivity of sky (-)

ACKNOWLEDGEMENT

This work was carried out as a contribution to the French National Research program PREBAT managed by the ADEME entitled RESSOURCES (Convention ADEME 0705C0076). The help from the partners: EDF R&D (R. Leberre, HBS-Technal (P. Lahbib, J. H. Fortier), Jacques Ferrier Architectes (O. Cornefert) is acknowledged.

REFERENCES

Chow T.T. 2003, Performance analysis of photovoltaic-thermal collector by explicit dynamic model, Solar Energy 75 (2003) 143-152

Chow T.T., A review on photovoltaic/thermal hybrid solar technology, Applied Energy 87 (2010) 365

European Commission 2010. Energy 2020 - A strategy for competitive, sustainable and secure energy, Brussels, Belgium, http://ec.europa.eu/energy/energy2020/energy2020_en.htm, accessed 2012

Gaillard L., Giroux S., Pabiou H., Ménézo C., Full scale experimentation of building integrated photovoltaic component for naturally ventilated double-skin configuration, Proceedings of Solaris 2012, Varanasi, India

Guiavarch A., Peuportier B., Photovoltaic collectors efficiency according to their integration in buildings, Solar Energy 80 (2006) 65

Guiot T., Boddaert S., Boillot B., Assoa Y.B., Gaillard L., Thermal behaviour of rooftop BIPV systems: an experimental approach, Proceedings 27th European Photovoltaic Solar Energy Conference (2012) p4136-4139

Ministère de l'Ecologie, du Développement Durable et de l'Energie 2012. Règlementation Thermique 2012, France, http://www.developpement-durable.gouv.fr/Chapitre-I-La-reglementation.html, accessed 09/2012

Neymark J., Girault P., Guyon G., Judkoff R., LeBerre R., Ojalvo J., Reimer P., The "ETNA Bestest" Empirical Validation Data Set, IBPSA BS05 proceedings, Montréal, Canada, (2005), pp839-846

Ong K.S., Chow C.C., Performance of a Solar Chimney, Solar Energy 74 (2003) 1-17

Sandberg M, Moshfegh B. 1998. Ventilated solar roof airflow and heat transfer investigation. Renewable Energy 15 (1998) 287-292

Scilab Enterprises, Scilab: Free and Open Source software for numerical computation [Software], available from: http://www.scilab.org (2012)

Zöllner A., Winter E.R.F., Viskanta R., Experimental studies of combined heat transfer in turbulent mixed convection fluid flows in double-skin-façades, International Journal of Heat and Mass Transfer 45 (2002) 4401